ADVANCED MATERIALS TECHNOLOGIES
www.advmattechnol.de

Functional Liquid Metal Nanoparticles Produced by Liquid-Based Nebulization

Shi-Yang Tang, Ruirui Qiao, Yiliang Lin, Yuhuan Li, Qianbin Zhao, Dan Yuan, Guolin Yun, Jinhong Guo, Michael D. Dickey, Tony Jun Huang, Thomas P. Davis, Kourosh Kalantar-Zadeh,* and Weihua Li**

Functional liquid metal nanoparticles (NPs), produced from eutectic alloys of gallium, promise new horizons in the fields of sensors, microfluidics, flexible electronics, catalysis, and biomedicine. Here, the development of a vapor cavity generating ultrasonic platform for nebulizing liquid metal within aqueous media for the one-step production of stable and functional liquid metal NPs is shown. The size distribution of the NPs is fully characterized and it is demonstrated that various macro and small molecules can also be grafted onto these liquid metal NPs during the liquid-based nebulization process. The cytotoxicity of the NPs grafted with different molecules is further explored. Moreover, it is shown that it is possible to control the thickness of the oxide layer on the produced NPs using electrochemistry that can be embedded within the platform. It is envisaged that this platform can be adapted as a cost-effective and versatile device for the rapid production of functional liquid metal NPs for future liquid metal-based optical, electronic, catalytic, and biomedical applications.

1. Introduction

Research on the production and application of micro-/nanosized particles of gallium liquid metal alloys, such as eutectic gallium indium (EGaIn, m.pt. 15.5 °C) and gallium indium tin (Galinstan, m.pt. −19 °C), is increasingly attracting attention. This is due to the unique properties possessed by such liquid metals including negligible vapor pressure and low toxicity compared to mercury, high electrical and thermal conductivities, and the ability to form a functional native oxide layer on the surface.[1] Numerous applications have been explored for micro/nanoparticles of such liquid metals in the fields of microfluidic systems,[2] soft electronics,[3] catalysts,[4] and biomedicines.[5] For example, due to their high electrical/thermal conductivities and reconfigurable surface property, EGaIn/Galinstan micro/nanoparticles have been embedded in microchannels or elastomers for constructing 3D electrodes,[2b] electrical interconnects,[3a,d,e] soft robots,[6] and heat dissipating systems.[3b] The presence of native gallium oxide layer on the surface of the particles allows for the formation of liquid metal/metal oxide structures that give them non-Newtonian rheological properties that allow the formation of stable nanoparticles (NPs).[4] Moreover, the research on using such liquid metal NPs for applications in biomedicine has shown great promises. For example, liquid metal NPs of gallium alloys, which are highly biocompatible, can undergo shape transformation upon the application of external stimuli, making them useful in targeted drug delivery systems with enhanced and controllable cargo releasing performance.[5a,b]

Dr. S.-Y. Tang, Q. Zhao, Dr. D. Yuan, G. Yun, Prof. W. Li
School of Mechanical, Materials, Mechatronic and Biomedical Engineering
University of Wollongong
Wollongong, NSW 2522, Australia
E-mail: shiyang@uow.edu.au; weihuali@uow.edu.au

Dr. R. Qiao, Dr. Y. Li, Prof. T. P. Davis
ARC Centre of Excellence in Convergent Bio-Nano Science and Technology
Monash Institute of Pharmaceutical Sciences
Monash University
Parkville, VIC 3052, Australia

Dr. Y. Lin, Prof. M. D. Dickey
Department of Chemical and Biomolecular Engineering
North Carolina State University
Raleigh, NC, USA

Prof. J. Guo
School of Communication and Information Engineering
University of Electronic Science and Technology of China
Chengdu 611731, China

Prof. T. J. Huang
Department of Mechanical Engineering and Materials Science
Duke University
Durham, NC 27708, USA

Prof. T. P. Davis
Department of Chemistry
University of Warwick
Gibbet Hill, Coventry CV4 7AL, UK

Prof. K. Kalantar-Zadeh
School of Chemical Engineering
University of New South Wales
Sydney, NSW 2052, Australia
E-mail: k.kalantar-zadeh@unsw.edu.au

The ORCID identification number(s) for the author(s) of this article can be found under https://doi.org/10.1002/admt.201800420.

DOI: 10.1002/admt.201800420

Top-down methods are commonly used for producing liquid metal microdroplets or NPs by overcoming the surface tension using disruptive shear induced by acoustic waves,[4a,5a,b,e,7] rotary tools,[8] or microfluidic devices.[9] The rapid formation of a thin oxide layer on the particles' surface helps in preventing coalescence back into the bulk materials.[1a] For the production of liquid metal NPs, high-power sonication probe systems have been the most commonly used for efficiently and promptly disrupting bulk liquid metals.[4,7a,c] However, commonly employed sonication probe systems are of high noise levels, lack controllability, they do not allow the implementation of specific configurations that help in regulating the process and also their intense power density can lead to instant dealloying and morphological for the produced liquid metal NPs.[4,7a] Furthermore, it is challenging to stabilize gallium-based liquid metal NPs within aqueous media as they are inclined to hydrolysis and oxidation, inducing aggregation after dealloying and forming gallium oxide nanostructures.[4,7a] Thiolated molecules are often used for stabilizing the liquid metal NPs.[1b,5a,b,7c] Unfortunately, thiol groups are prone to oxidation and are often not suitable for direct use in biological systems as they foul readily.

Thus, we sought to design a platform that is of reduced technological complexity, highly efficient, integrated, noise-free, small-in-size, and versatile for the production of stable, highly controllable and functional liquid metal NPs. We report a mini ultrasonic platform to efficiently nebulize EGaIn liquid metal within aqueous media for the production of liquid metal NPs, and we also characterize their size distributions. We discovered that this platform forms particles by inducing vapor cavities and collapsing them at the liquid metal–medium interface, which is different from conventional acoustic systems where strong shear is applied to disrupt the liquid metal. Leveraging the versatility of this platform, we investigated grafting of various molecules to the NPs to yield both stability and stealth properties, and examined the cytotoxic effects of the NPs on cells. We also studied the capability of this miniaturized platform for controlling the thickness of the oxide shell on the produced NPs using electrochemical components added onto the system.

2. Results and Discussion

The mini ultrasonic platform is illustrated in **Figure 1**A. A low-cost commercially available ultrasonic mist maker equipped with a lead zirconate titanate (PZT) transducer (resonant frequency of ≈1.71 MHz) was utilized to produce EGaIn NPs. The top surface of the transducer has a layer of ceramic glaze for protection. The mist maker has an oscillator that converts the DC voltage supply into a 1.71 MHz AC signal to drive the PZT transducer with power consumption less than 12 W. A stainless steel tube with the length, inner diameter, and thickness of 30, 10, and 1 mm, respectively, was inserted into the oscillator as a medium container to allow for the production of EGaIn NPs upon the activation of the transducer (Figure 1A). The stainless steel tube was passivated using a 20% nitric acid solution at 50 °C for 30 min before using to avoid any contamination and chemical reaction. We chose to use the stainless steel tube as the container due to its simple fabrication process (by lathing) and excellent ability to dissipate heat. A 5 mL test tube was used as the cap to avoid spilling/leaking during production and to collect the final NP suspension (Figure 1B); the enclosed platform was submerged into tap water to activate the AC signal generator and avoid overheating during the production process.

To understand the production mechanism, we first conducted a numerical simulation to investigate the distribution of acoustic surface displacement on the PZT transducer, as shown in Figure 1C. The top and bottom images for the transducer are given in Figure S1A (Supporting Information). Figure 1C shows the center of the transducer has the maximum displacement at the resonant frequency, and this is evidenced by our experimental results conducted using the transducer to nebulize a droplet of water, as shown in Figure S1B (Supporting Information). Upon the activation of the transducer, we observed the immediate jetting of water at the center, and later formation of a cone-shaped droplet (Figure S1B, Supporting Information), indicating that the acoustic energy was accumulated at the center of the transducer.

The cross-sectional schematic of the EGaIn NP production system is given in Figure 1D, in which NPs of EGaIn can be produced after activating the transducer at the resonant frequency. We added 300 µL of EGaIn and 2 mL of the aqueous suspending medium into the platform. A conventional sonication probe/bath fractures the bulk liquid metal into NPs by the strong oscillating shear forces induced by acoustic waves.[7a,c] In contrast, we did not observe severe turbulence upon the activation of the transducer, as shown in Figure 1E (also see Movie S1, Supporting Information); this indicates that the production mechanism could be different from conventional methods that use acoustics. We also rule out capillary instabilities since such a phenomenon is commonly observed at low ultrasonic frequencies (<100 kHz).[10] In Movie S1 (Supporting Information), we can see the generation of NPs comes along with the production and collapse of bubbles on the surface of the EGaIn droplets. Therefore, we believe the liquid metal is nebulized within the medium and the production mechanism can be explained using the cavitation hypothesis,[10] as shown in Figure 1D. Vapor cavities of water can be generated within the slip layer between the EGaIn droplet and the surface of transducer by acoustic waves; next, the bubbles move upward into the EGaIn droplet and eventually collapse at the EGaIn–solution interface, liberating EGaIn NPs into the surrounding suspending medium. This phenomenon is also similar to the case of forming nanoemulsions/NPs via bubble-bursting at a liquid–liquid interface.[11]

Benefiting from the versatility of this platform, we investigated the use of various grafting molecules, including brushed polyethylene glycol (bPEG, MW of 20 kDa), poly(methyl vinyl ether-*alt*-maleic anhydride) (PMVEMA, MW of 216 kDa), poly(styrene-*co*-maleic anhydride) (PSMA, MW of 224 kDa), and oleic acid (OA), for coating and stabilizing the EGaIn NPs electrostatically or sterically in water. Similar to our previous work,[9b] the bPEG polymers used here have a brush-like structure with carboxyl and trithiocarbonate termini, where the trithiocarbonate groups were used as the surface anchoring compartments for EGaIn NPs. PMVEMA and PSMA polymers contain maleic anhydride groups, which can be hydrolyzed

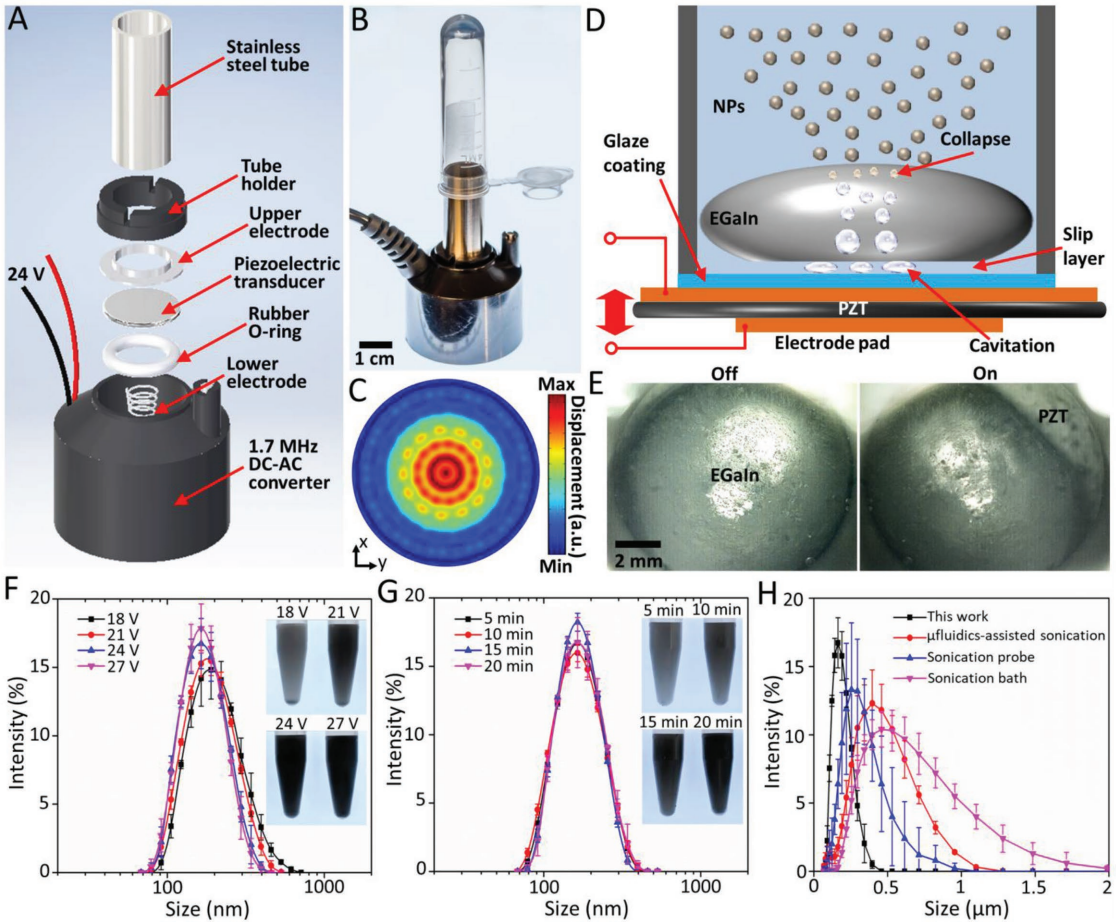

Figure 1. Production of EGaIn nanoparticles using the mini ultrasonic platform. A) Exploded schematic of the platform. B) Actual image of the assembled device. C) Numerical simulation of the displacement on the top of the PZT transducer upon the application of a 1.71 MHz signal. D) Schematic illustrating the mechanism for producing EGaIn nanoparticles. E) Snapshots showing the EGaIn droplet within the device before and after activating the transducer. F) Hydrodynamic size distributions for the PMVEMA grafted NPs obtained using different input voltages; the inset shows the image of the EGaIn NP suspensions. G) Hydrodynamic size distributions of the NPs produced using different production time, the input voltage was kept at 24 V; the inset shows the image of the EGaIn NP suspensions. H) Hydrodynamic size distributions of the EGaIn NPs produced using the ultrasonic device presented in this paper in comparison with other methods.

to carboxylic acid in water. We hypothesize that the hydrolyzed PMVEMA and PSMA polymers can bind to the surface of EGaIn NPs through the carboxylic groups, and meanwhile stabilizing the NPs due to the electrostatic repulsion from the strong negative charge, therefore, enabling one-step stabilization and functionalization process during the production process.

Using the PMVEMA polymer grafted NPs as an example, upon adding 2 mL of the polymer solution (concentration of 2.5 mg mL^{-1}) and activating the transducer for 20 min, this platform is capable of producing stable PMVEMA-grafted EGaIn NPs with sizes ranging from tens to a few hundreds of nanometers, where the size distribution and concentration of the NPs can be controlled by changing the input DC voltage. We placed the NP suspensions in the steady state for 20 min after the production and take 1 mL of the supernatant for measurement and characterization. We find that the concentration of the NPs can be increased from ≈0.5 to ≈5 mg mL^{-1} by increasing the input voltage from 18 (≈5 W power consumption) to 27 V (≈11 W power consumption). This is visually seen by the decreased transparency of the NP suspensions obtained using higher input voltages as presented in the inset of Figure 1F. In addition, the dynamic light scattering (DLS) measurements show that the peak of the hydrodynamic size distribution for the NPs shifts to smaller sizes when activating the transducer using larger voltages, reducing from ≈200 to ≈160 nm when the voltage increases from 18 to 27 V, as shown in Figure 1F. Interestingly, despite the increased concentration of the NPs obtained by activating the transducer for a longer time using the same input voltage (Figure 1G inset), we did not observe any noticeable difference for the size distributions of the NPs, as shown in Figure 1G. This further suggests that the formation of NPs is not due to the continuous shear forces induced by acoustic waves, which can lead to a smaller size of NPs by extending the sonication time.[4a]

Breaking of the bulk liquid metal into microdroplets or NPs is a result of the competition between destructive (shear forces) and cohesive (surface tension) forces on the liquid–liquid interface. The capillary number is a ratio of viscous forces to interfacial forces and is calculated as $Ca = \mu V/\gamma$, where μ and V are

the dynamic viscosity and characteristic velocity of the polymer solution, respectively, and γ is the interfacial tension between liquid metal and the solution. The size of liquid metal droplets produced varies inversely with the *Ca*.[9a] Despite the claim that sub-micrometer to nanosized particles of low-melting-point metal such as bismuth can be produced with a narrow size distribution simply by stirring at a speed of few hundreds of rpm,[12] it is very unlikely to happen in our case as the *Ca* is too small (≈0.02) even we applied a high stirring speed of 1600 rpm, as shown in Figure S2A (Supporting Information). Our previous study shows that even with a large *Ca* of ≈2 within a flow-focusing microfluidic device, only large liquid metal microdroplets with a diameter of ≈100 µm can be produced.[9a] As a result, we only observed the production of large nonspherical liquid metal droplets (major axis of ≈200 µm) after vigorously stirring the bulk liquid metal within the polymer solution at a high speed of 1600 rpm (see Figure S2A, Supporting Information). We also tried to increase the *Ca* using a much more viscous liquid such as polydimethylsiloxane (PDMS); however, we could only break the liquid metal into polydispersed droplets with the diameter of tens of micrometers, as shown in Figure S2B (Supporting Information). The polydispersity of the produced liquid metal droplets using such a stirring method is due to the large Reynolds number ($\approx 2 \times 10^4$) at the high stirring speed (1600 rpm). Consequently, the flow is rather turbulent and no constant shear can be induced to evenly break the bulk liquid metal into monodispersed microdroplets or NPs.

We further compared the production of liquid metal NPs using this ultrasonic device with other methods, including sonication using bath or probes, as well as microfluidics-assisted sonication.[9b] For the production using a sonication bath, an 8 mL glass vial contains 2 mL polymer solution and 300 µL EGaIn was sonicated using a 60 W sonication bath for 20 min. For the production using a sonication probe, an 8 mL glass vial contains 2 mL polymer solution and 300 µL EGaIn was sonicated using a sonication probe with a 90 W output power for 20 min. We placed the NP suspensions in a steady state for 20 min after production and take 1 mL of the supernatant for the DLS measurements. We discovered that the device presented in this paper can produce NPs with a size distribution that is narrower and at least two times smaller in comparison with other methods using less power, and also the distribution of the size is always smaller than 500 nm while other methods may produce a large portion of particles in microsized dimensions, as detailed in Figure 1H.

We operated the ultrasonic device with an input voltage of 24 V for 20 min, and our method was able to produce stable and stealthy EGaIn NPs grafted by bPEG, PMVEMA, or PSMA polymer directly within an aqueous solution. As an example, **Figure 2**A shows the scanning electron microscopy (SEM) image for the PMVEMA-grafted EGaIn NPs. We measured the zeta potentials for the NPs with or without the polymer grafting, as shown in Figure 2B. The zeta potential of EGaIn NPs without grafting is low and therefore, induces aggregation rapidly after production.[9b] A neutral surface charge was observed for NPs grafted with bPEG, indicating that bPEG polymer is able to sterically stabilize the NPs in water. We obtained large negative zeta potentials for the cases of PMVEMA (–55.3 ± 5.6 mV) and PSMA (–53.9 ± 5.2 mV) grafted NPs, indicating that part of the hydrolyzed polymer long chain was able to bind to the surface of EGaIn NPs via the ionized carboxyl groups, and meanwhile stabilizing them electrostatically and sterically within water (Figure 2B inset). Such a conjugation/stabilization method is similar to the case of using poly(vinyl alcohol) to prevent the merging of EGaIn microdroplets produced using a microfluidic platform.[13] Surprisingly, we found that the platform also allowed us to use OA as the grafting molecule despite the fact that OA is immiscible in water. This was achieved by adding 50 µL of OA into the 2 mL deionized (DI) water within the platform, and micelles of OA were produced together with EGaIn NPs by acoustic waves created upon the activation of the transducer. We believe that the produced EGaIn NPs were

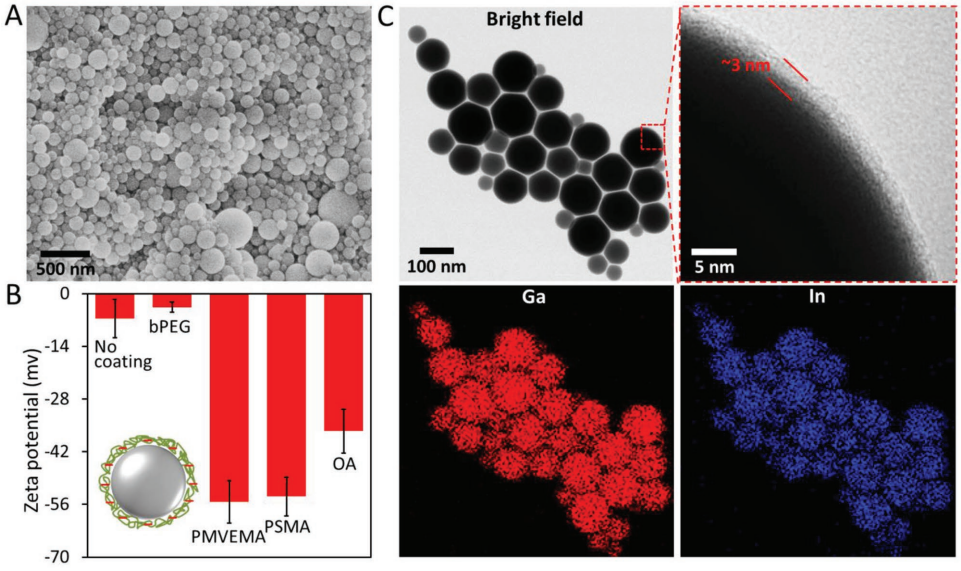

Figure 2. Characterization of the produced EGaIn NPs. A) SEM image of the PMVEMA grafted EGaIn NPs. B) Zeta potentials for the EGaIn NPs with/without grafting. C) TEM images and EDS mapping of the PMVEMA grafted EGaIn NPs.

attached to the hydrophilic carboxyl head of OA molecules, and their hydrophobic tail might be interacting with the free OA by hydrophobic interactions. After 20 min of production, the NPs suspension was centrifuged to remove excess OA, and the NPs were washed and resuspended in DI water. For dispersion of OA-coated NPs in water, the carboxyl group of free OA needs to be ionized, and this was evidenced by the strong negative zeta potential (-36.5 ± 5.9 mV) measured for the OA-grafted EGaIn NPs (Figure 2B).

We further obtained transmission electron microscopy (TEM) images and energy-dispersive X-ray spectroscopy (EDS) mapping for the EGaIn NPs to examine the uniformity of gallium and indium distribution. Figure 2C shows the example of PMVEMA-grafted NPs, from which we can see a thin layer of oxide formed on the NP surface, and the grafting polymer is not obvious due to its small thickness and similar contrast to the background (zoomed-in image of Figure 2C). Despite that the surface composition of gallium-indium alloys is dominated by indium in high vacuum, the shell of the alloy primarily consists of gallium oxide because indium is less prone to be oxidized and thermodynamically gallium oxide is preferential over indium oxide.[14] The growth of the gallium oxide could be controlled through thiolation,[15] thermal oxidation,[16] or electrochemistry.[17] Thiolation can mitigate (but not eliminate) the growth of gallium oxide.[15] For thermal oxidation, the thickness, texture, and roughness of the oxide layer is temperature-dependent that it grows thicker and rougher with increasing temperature.[16] While in electrochemistry, the oxide skin becomes thicker with increasing oxidative potential.[17] To further examine the thickness of the oxide layer and the grafted PMVEMA, we conducted EDS mapping for a single NP using a TEM grid coated with a lacey carbon film, as shown in Figure S3 (Supporting Information), from which we discovered that the thickness of the oxide layer and the grafted polymer are ≈3 and ≈2.5 nm, respectively. No diffraction pattern was observed from the convergent-beam electron diffraction (CBED) measurement (see Figure S4, Supporting Information), indicating that the core of NPs is liquid. The EDS mapping indicates a uniform distribution of gallium and indium within the NPs (Figure 2C). The temperature measured for the suspension was below 40 °C when activating the transducer less than 30 min (see Figure S5, Supporting Information); this minimized the chance of inducing dealloying and morphological transformation observed for liquid metal NPs caused by oxidation after exposing to a high temperature (≈70 °C).[7a] The use of polymers and OA for stabilizing the produced EGaIn nanoparticles represents a significant advance in comparison to previous reports that use thiol-functionalized molecules for stabilization.[1b,5a,b] In comparison, our approach for nanoparticle anchoring avoids the use of thiol groups that induce unpleasant odors and are prone to oxidation reactions and as a consequence, inducing fouling within biological systems.

After obtaining the stable NPs suspensions, we further studied their stability within water over a longer period of time (120 h). We have previously showed that bPEG-grafted EGaIn NPs are prone to oxidization and formation of gallium oxide nanodisks within 48 h without the presence of an antioxidant such as trisodium citrate.[9b] Interestingly, for the case of PMVEMA-grafted NPs, we found that the NPs suspension is relatively stable (can be resuspended) but became more transparent after 120 h, as shown in **Figure 3**A. We obtained the TEM image for the EGaIn NPs 120 h after production (see Figure 3A) and observed the formation of core–shell structured NPs. Most of the NPs have a thick layer of gallium oxide shell (10–20 nm) and an indium-rich core, as evidenced by the EDS spectrum. The CBED results indicate that the core of the NPs became solid (see Figure S6, Supporting Information), and this can be attributed to the dealloying process induced by the gradual oxidation of metallic gallium on the surface, increasing the content of indium and solidifying the core. In addition, we also observed the formation of gallium oxide nanodisks (see the TEM image in Figure 3A), as evidenced by the EDS spectrum given in Figure S7 (Supporting Information). The X-ray diffraction (XRD) and X-ray photoelectron spectroscopy (XPS) spectra given in Figure S8 (Supporting Information) show that the oxide layer on the NPs was mainly composed of α-Ga_2O_3 at 0 h, and it gradually became thicker and transformed into GaOOH 120 h after production. Similar results were obtained for PSMA-grafted NPs. We believe that the loss of liquidity and formation of gallium oxide nanodisks may contribute to the enhanced transparency of the suspension, as evidenced by the experiments conducted using pure gallium instead of EGaIn, where the gallium NPs were oxidized and the suspension became transparent 120 h after the production, as shown in Figure S9 (Supporting Information).

On the contrary, the OA-grafted NPs are very stable with no change of the particle concentration and morphology observed over the period of 120 h, as shown in Figure 3B. The CBED measurements prove that the NPs were still liquid and the EDS spectrum indicates no hydrolysis and oxidation occurred for the NPs (Figure 3B). Such an unprecedented stability is due to the formation of an insulation layer from the hydrophobic tails of OA (see the inset of the EDS spectrum). Our DLS measurements show that the peak of the distribution for PMVEMA-grafted NPs shifted toward the larger size by ≈40 nm due to the formation of nanodisks after 120 h (see Figure 3C), while no shift of the peak was observed for OA-grafted NPs. We further compared the UV–vis spectra for the suspensions of PMVEMA and OA-grafted NPs 120 h after production, as shown in Figure S10 (Supporting Information), for which no peak was detected for OA-coated NPs while a broad peak at ≈330 nm was observed for the case of PMVEMA. This further confirms the formation of solid indium NPs.[18]

Such an excellent stability and the presence of carboxyl functioning groups for OA-grafted NPs can allow us to conduct further functionalization. We conducted a proof-of-concept experiment to conjugate Rhodamine 123 (R123) fluorescent dye to the OA-grafted EGaIn NPs, where a 1-ethyl-3-(3- dimethylaminopropyl)carbodiimide (EDC)-mediated crosslinking method was used. Briefly, EDC (final concentration of 1×10^{-3} M) was first added into 3 mL of the NPs suspension to react with carboxylic acid groups, and then the unreacted EDC was removed using dialysis tubing (2000 Da MWCO). Next, we added 5 µL of R123 solution (concentration of 10 mg mL^{-1}) into the NP suspension to allow for the formation of amide bonds between the R123 and the NPs. The conjugated NPs were later washed with dialysis tubing (2000 Da MWCO) and we examined the functionalization using a fluorescence spectrophotometer.

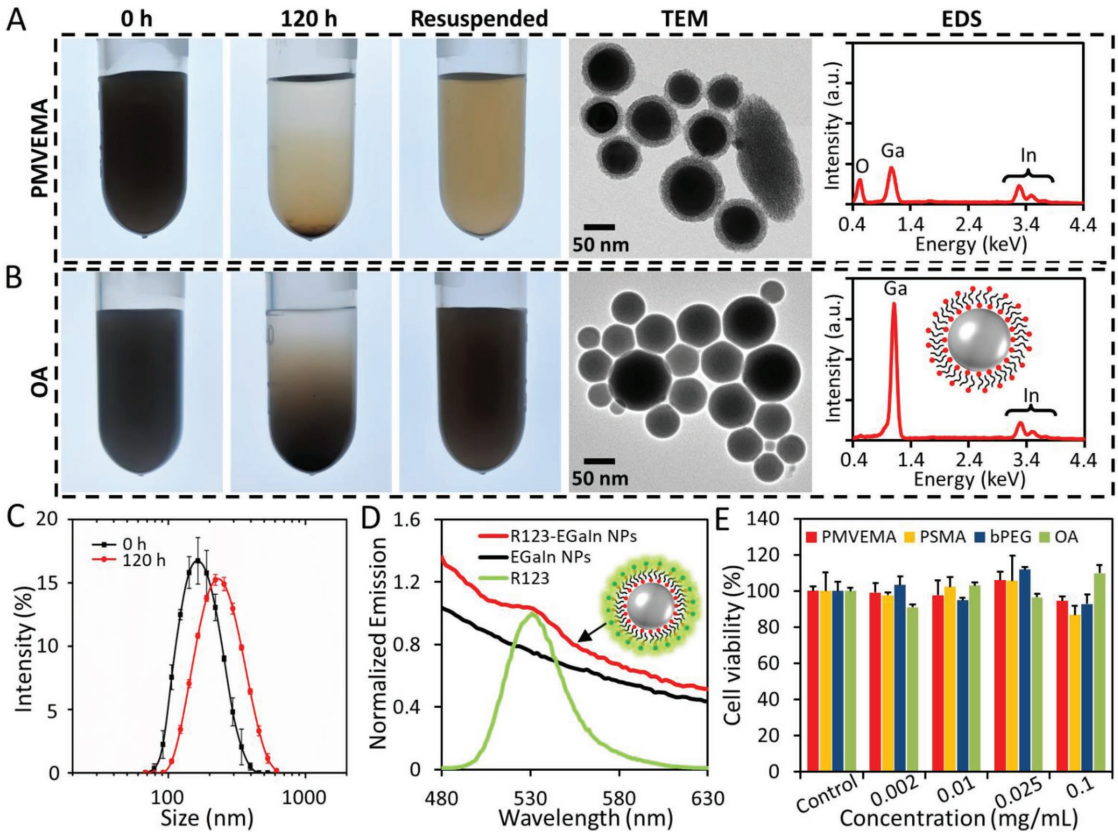

Figure 3. Stability of the NP suspensions. EGaIn NP suspension, TEM image, and EDS spectrum for NPs grafted using A) PMVEMA, and B) OA over the duration of 120 h. C) DLS size distribution for PMVEMA grafted NPs 0 and 120 h after production. D) Normalized emission intensity for the R123 solution, bare EGaIn NP, and R123-conjugated EGaIn NP suspensions. E) The effect of concentration for NPs grafted with different molecules on the survival rates of MCF-7 cells.

The obtained emission spectra for the R123 solution, bare EGaIn NP suspension, and R123-conjugated EGaIn (R123-EGaIn) NP suspension, are given in Figure 3D. The R123 solution has an emission peak at ≈530 nm and the presence of such a peak for the spectrum obtained with the R123-conjugated EGaIn NP suspension clearly proved the success of functionalization. The bright field and fluorescent images for the dry R123-conjugated EGaIn NP cluster are given in Figure S11 (Supporting Information), in which we can clearly see the bright green-colored fluorescent light emitted from the NPs. Such a functionalization process for EGaIn NPs is only possible for a very stable suspension where no oxidation and aggregation of NPs should occur due to the time-consuming particle washing process using dialysis tubing (a few days), thus, the use of OA for grafting EGaIn NPs within our innovative platform certainly represents a significant advance in comparison to previously reported methods.

We envisioned that such a stable EGaIn NP system may enable various bioapplications and therefore, we further examined the cytotoxicity of EGaIn NPs grafted with different molecules on MCF-7 cell line using the Alamar Blue assay (see the Experimental Section for details). Figure 3E shows the viability of the cells upon the 24 h exposure to the NPs with different concentrations; we observed that the viability of MCF-7 cells slightly decreased as the concentration of the NPs was increased to 0.1 mg mL^{-1} for the cases of PMVEMA, PSMA, and bPEG-grafted NPs, while no significant cytotoxicity was observed for OA-grafted NPs.

Based on our understanding of the NPs production mechanism elaborated in Figure 1, where the NPs were produced due to the collapse of the cavities at the EGaIn–solution interface, we hypothesized that the thickness of the oxide shell on the NPs can be controlled electrochemically in this platform upon the application of a reductive or oxidative potential to the bulk EGaIn droplet during the production.[19] We conducted a proof-of-concept experiment to verify our hypothesis, and the schematic and actual image depicting the experimental setup is given in **Figure 4**A,B, respectively. We electrochemically reduced/oxidized the surface of EGaIn via a pair of copper electrodes in contact with the EGaIn droplet and the surrounding suspending medium, respectively. In this study, we used a PMVEMA solution as the suspending medium due to its relatively high electrical conductivity (≈2 mS cm^{-1}). We first examined the size distributions of the NPs at different reductive/oxidative voltages, as shown in Figure 4C. Upon the activation of the transducer and applying a −5 V reductive potential to the liquid metal, we observed a slight peak shift of the size distribution toward larger sizes. This could probably be due to the increased surface tension of EGaIn after removing the oxide layer electrochemically.[7b] We also observed a shift of the size

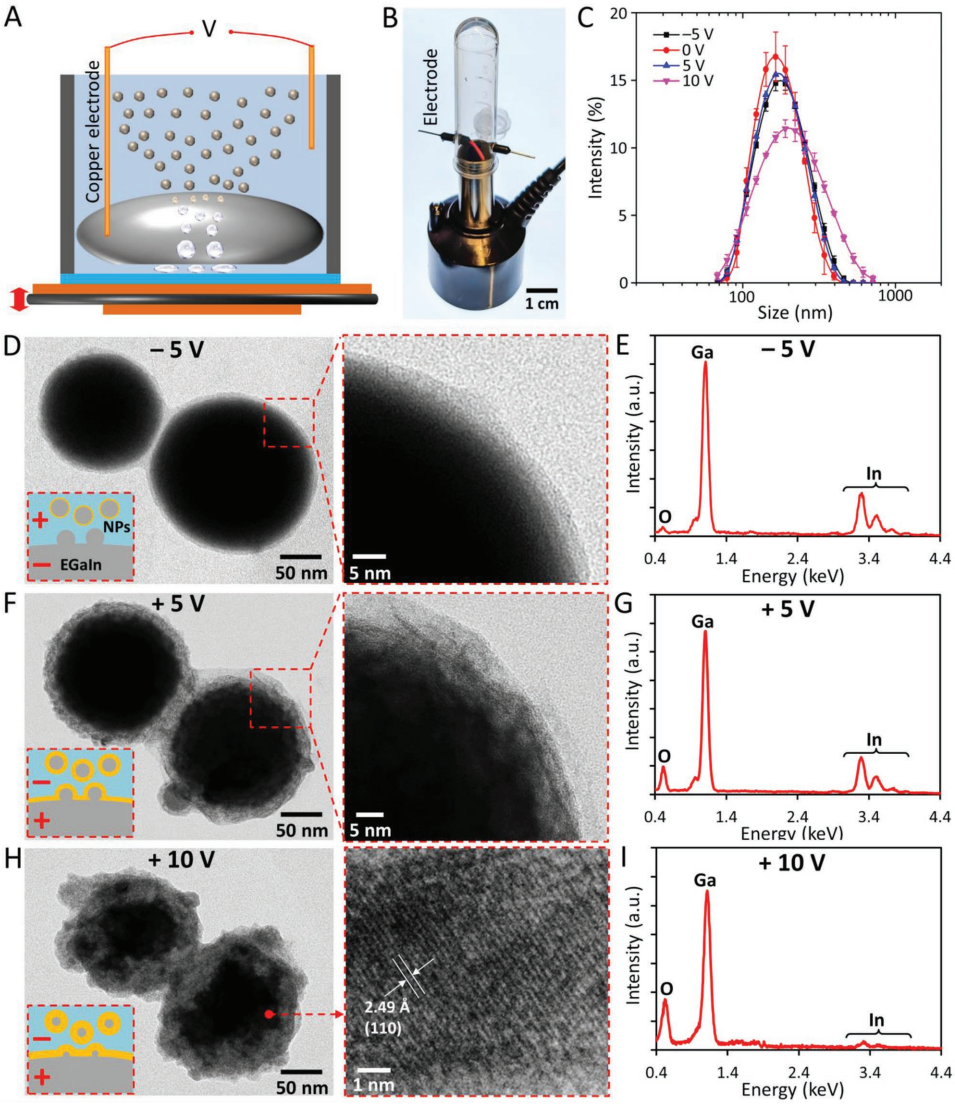

Figure 4. Electrochemically control over the thickness of the oxide layer on the NPs. A) Schematic and B) actual image of the experimental setup with electrochemical control over the thickness of the oxide shell on the produced NPs. C) Hydrodynamic size distributions of the NPs produced when applying different reductive/oxidative potentials. TEM images and EDS spectrum for the NPs produced with the application of a D,E) −5 V, F,G) +5 V, and H,I) +10 V with respect to the surrounding medium. The insets show the schematics of the NPs production process.

distribution toward larger values when an oxidative potential was applied during the production process, and the size distribution was broadened after applying larger oxidative potentials (Figure 4C). This can be attributed to the formation of thicker and solid oxide layer that may hinder the formation of EGaIn NPs from the surface.

When we investigate the produced NPs using TEM, we found that for the case of the NPs produced with the application of a −5 V reductive potential, no obvious difference was observed for the NPs in comparison to the case without applying a voltage, as shown in Figure 4D. The inset of Figure 4D shows the schematic of the NPs production, where the produced NPs can be oxidized by the oxygen dissolved into the PMVEMA solution. The EDS spectrum given in Figure 4E indicates the proper composition of gallium and indium within the NPs with minimum oxidation occurred.

Interestingly, a thick oxide shell (≈15 nm) was formed on the obtained NPs when we applied a +5 V oxidative potential to the EGaIn droplet during the production, as shown in Figure 4F. The oxide shell is mainly composed of α-Ga_2O_3, as evidenced by the XRD and XPS spectra given in Figure S12 (Supporting Information). We believe this is due to the fact that such a thick oxide layer was already formed on the surface of liquid metal before liberating NPs, and upon the collapse of cavities that NPs with a thick oxide layer were produced, as depicted in Figure 4F inset. The EDS spectrum given in Figure 4G confirms the oxidation with the appearance of the oxygen peak. When we further increase the oxidative potential to +10 V, we found that the produced NPs were heavily oxidized and became nonspherical, as shown in Figure 4H. Such heavily oxidized NPs lost their liquidity, as indicated by the diffraction pattern given in the magnified image in Figure 4H. The

increase in the intensity of the oxygen peak, and the decrease in the intensity of the indium peaks (see Figure 4I) clearly show the formation of gallium oxide and only a small trace amount of indium exists within the NPs. This is probably due to the fact that gallium is much more prone to oxidation compared to indium and therefore, only a small amount of gallium-indium alloy can be incorporated into the produced NPs (see the inset of Figure 4H). The observed formation of a thick oxide layer on the surface of NPs explains the shift of the size distribution toward the larger sizes when oxidative potentials were applied (see Figure 4C).

Following our initial studies on the EGaIn NPs produced using this platform, we also found that due to the smaller and narrower size distribution of the produced NPs in comparison to previous reports,[9b] the optical properties of the EGaIn NP suspension can be modified after forming nanosized liquid metal marbles[20] coated with silver (Ag) NPs, as shown in Figures S13 and S14 (Supporting Information). We discovered that the AgNP coating on the surface can introduce a strong surface plasma resonance due to the strong interaction of the AgNPs with light. This interaction results in strong scattering and absorption properties, leading to a significant absorption peak at ≈418 nm for the nanosized liquid metal marbles (see Figures S13 and S14, Supporting Information).

3. Conclusion

In summary, we developed a novel ultrasonic platform to nebulize liquid metal within aqueous media for the versatile and efficient production of functional EGaIn liquid metal NPs. We fully characterized the size distribution of NPs and discovered that the median diameter of NPs can be tuned by the magnitude of the applied voltage and not by increasing the process duration. We discovered that various polymers and oleic acid can be directly used in this platform for grafting the surface of EGaIn liquid metal to stabilize the produced NPs in aqueous media. Based on the excellent stability of the produced EGaIn NPs, we showed that the produced NPs can be further functionalized without inducing oxidation and aggregation of the NPs. We also demonstrated that the grafted NPs have little or no effect on the viability of MCF-7 cells at the concentration of 0.1 mg mL^{-1}. Most importantly, this platform allows us to electrochemically control the thickness of the oxide shell on the produced NPs. As such, the simplicity and versatility of the ultrasonic platform, together with the multifaceted functionality of the produced EGaIn NPs, possess the vast potential to enable a new horizon for developing future liquid metal-based optical, electronic, catalytic, and biomedical applications.

4. Experimental Section

Chemical Preparation: PMVEMA (MW of 216 kDa), PSMA (MW of 224 kDa), oleic acid, dialysis tubing (2000 Da MWCO), Rhodamine 123, EDC, and silver nitrate ($AgNO_3$) were purchased from Sigma Aldrich, USA. Ultrasonic mist makers were purchased from AGPTEK, USA. PMVEMA and PSMA polymer solutions were prepared by dissolving 50 mg PMVEMA and PSMA into 20 mL of DI water, respectively (final concentration of 2.5 mg mL^{-1}), and mixed for 24 h to allow for the full hydrolysis; the pH of the solutions was ≈3.0.

Polymer Synthesis: bPEG (MW of 20 kDa) was synthesized using the reversible addition-fragmentation chain transfer (RAFT) polymerization techniques.[21] Briefly, a solution of RAFT agent, 2, 2′-azobis(isobutyronitrile) (AIBN), and monomers in dioxane was added to a polymerization ampoule. The solution was degassed by sparging with nitrogen for 20 min and the ampoule was sealed under nitrogen, while the reaction was stirred at 65 °C. Samples were then taken for 1HNMR spectroscopy and gel permeation chromatography (GPC) analysis. The bPEG solution was prepared by adding 50 mg of the bPEG into 10 mL DI water.

Alamar Blue Assay: MCF-7 (human breast cancer cell line, ATCC) were grown in Dulbecco's modified Eagle media (DMEM) culture media with 10% fetal bovine serum (FBS). MCF7 cells (1×10^4 cells/well) were exposed to materials (0.002, 0.01, 0.025, and 0.1 mg mL^{-1}) for 24 h in 96-well plates, with the final volume of 100 µL. Cell culture medium was used as a control. After exposure, the suspensions were removed and the cells were incubated with 10% Alamar Blue (Invitrogen) for 4 h at 37 °C. A microplate reader (CLARIOstar, BMG LABTECH) was used to read the fluorescence at 500 nm excitation and 530 nm emission. Background values (10% Alamar Blue in cell culture medium) were subtracted from each well and the average fluorescent intensity of the triplicates was calculated.

Characterization: SEM images were obtained using a JEOL JSM-7500FA scanning electron microscope. TEM images were obtained using a JEOL JEM-2011 transmission electron microscope. EDS maps were measured using JEOL JEM-ARM200f scanning transmission electron microscope (STEM). A zeta-sizer (Zetasizer Nano ZS, Marvern Instrument, USA) was used to measure the size distribution of the obtained EGaIn nanoparticles. The concentration of the EGaIn nanoparticles was measured by weighing the dried suspensions. UV–vis spectra were obtained using a UV–vis spectrophotometer (Uv-5200Pc, Metash instrument Co., Ltd., China). The fluorescent emission spectra were obtained using a fluorescence spectrophotometer (Cary Eclipse 500, Agilent Technologies, USA). XRD (MMA, GBC Scientific Equipment LLC, Hampshire, IL) was used to evaluate the composition of the oxide layer. XPS spectra were obtained using a PHOIBOS 100 Analyser from SPECS, Berlin, Germany; Al Kα X-rays.

Supporting Information

Supporting Information is available from the Wiley Online Library or from the author.

Acknowledgements

S.-Y.T. and R.Q. contributed equally to this work. S.-Y.T. is the recipient of the Vice Chancellor's Postdoctoral Research Fellowship funded by the University of Wollongong. T.P.D. and R.Q. were supported by the Australian Research Council Centre of Excellence in Convergent Bio-Nano Science and Technology (Project No. CE140100036). M.D.D. gratefully acknowledges support from the NSF (CMMI-0954321) and NSF Research Triangle MRSEC on Programmable Soft Matter (DMR-1121107). The authors acknowledge use of the facilities and the assistance of Dr. David Mitchell at the UOW Electron Microscopy Centre.

Conflict of Interest

The authors declare no conflict of interest.

Keywords

EGaIn, functional material, liquid metal, nanoparticle, nebulization

Received: September 5, 2018
Revised: October 5, 2018
Published online:

[1] a) M. D. Dickey, *ACS Appl. Mater. Interfaces* **2014**, *6*, 18369; b) L. R. Finkenauer, Q. Lu, I. F. Hakem, C. Majidi, M. R. Bockstaller, *Langmuir* **2017**, *33*, 9703; c) T. Liu, P. Sen, C.-J. Kim, *J. Microelectromech. Syst.* **2012**, *21*, 443.

[2] a) K. Khoshmanesh, S.-Y. Tang, J. Y. Zhu, S. Schaefer, A. Mitchell, K. Kalantar-Zadeh, M. D. Dickey, *Lab Chip* **2017**, *17*, 974; b) S.-Y. Tang, J. Zhu, V. Sivan, B. Gol, R. Soffe, W. Zhang, A. Mitchell, K. Khoshmanesh, *Adv. Funct. Mater.* **2015**, *25*, 4445; c) Q. Wang, Y. Yu, J. Liu, *Adv. Eng. Mater.* **2018**, *20*, 1700781.

[3] a) Y. Lin, C. Cooper, M. Wang, J. J. Adams, J. Genzer, M. D. Dickey, *Small* **2015**, *11*, 6397; b) M. D. Bartlett, N. Kazem, M. J. Powell-Palm, X. Huang, W. Sun, J. A. Malen, C. Majidi, *Proc. Natl. Acad. Sci. USA* **2017**, *114*, 2143; c) Q. Wang, Y. Yu, J. Yang, J. Liu, *Adv. Mater.* **2015**, *27*, 7109; d) Y. Chen, T. Zhou, Y. Li, L. Zhu, S. Handschuh-Wang, D. Zhu, X. Zhou, Z. Liu, T. Gan, X. Zhou, *Adv. Funct. Mater.* **2018**, *28*, 1706277; e) L. Tang, S. Cheng, L. Zhang, H. Mi, L. Mou, S. Yang, Z. Huang, X. Shi, X. Jiang, *iScience* **2018**, *4*, 302.

[4] a) W. Zhang, J. Z. Ou, S.-Y. Tang, V. Sivan, D. D. Yao, K. Latham, K. Khoshmanesh, A. Mitchell, A. P. O'Mullane, K. Kalantar-zadeh, *Adv. Funct. Mater.* **2014**, *24*, 3799; b) N. Syed, A. Zavabeti, M. Mohiuddin, B. Zhang, Y. Wang, R. S. Datta, P. Atkin, B. J. Carey, C. Tan, J. van Embden, J. Z. Ou, T. Daeneke, K. Kalantar-zadeh, *Adv. Funct. Mater.* **2017**, *27*, 1702295.

[5] a) S. A. Chechetka, Y. Yu, X. Zhen, M. Pramanik, K. Pu, E. Miyako, *Nat. Commun.* **2017**, *8*, 15432; b) Y. Lu, Q. Hu, Y. Lin, D. B. Pacardo, C. Wang, W. Sun, F. S. Ligler, M. D. Dickey, Z. Gu, *Nat. Commun.* **2015**, *6*, 10066; c) Y. Yu, E. Miyako, *iScience* **2018**, *3*, 134; d) X. Sun, B. Yuan, W. Rao, J. Liu, *Biomaterials* **2017**, *146*, 156; e) Y. Lu, Y. Lin, Z. Chen, Q. Hu, Y. Liu, S. Yu, W. Gao, M. D. Dickey, Z. Gu, *Nano Lett.* **2017**, *17*, 2138.

[6] E. J. Markvicka, M. D. Bartlett, X. Huang, C. Majidi, *Nat. Mater.* **2018**, *17*, 618.

[7] a) Y. Lin, Y. Liu, J. Genzer, M. D. Dickey, *Chem. Sci.* **2017**, *8*, 3832; b) S.-Y. Tang, B. Ayan, N. Nama, Y. Bian, J. P. Lata, X. Guo, T. J. Huang, *Small* **2016**, *12*, 3861; c) J. N. Hohman, M. Kim, G. A. Wadsworth, H. R. Bednar, J. Jiang, M. A. LeThai, P. S. Weiss, *Nano Lett.* **2011**, *11*, 5104.

[8] a) S. Çınar, I. D. Tevis, J. Chen, M. Thuo, *Sci. Rep.* **2016**, *6*, 21864; b) I. D. Tevis, L. B. Newcomb, M. Thuo, *Langmuir* **2014**, *30*, 14308.

[9] a) S.-Y. Tang, I. D. Joshipura, Y. Lin, K. Kalantar-Zadeh, A. Mitchell, K. Khoshmanesh, M. D. Dickey, *Adv. Mater.* **2016**, *28*, 604; b) S.-Y. Tang, R. Qiao, S. Yan, D. Yuan, Q. Zhao, G. Yun, T. P. Davis, W. Li, *Small* **2018**, *14*, 1800118.

[10] D. Kirpalani, F. Toll, *J. Chem. Phys.* **2002**, *117*, 3874.

[11] a) J. Feng, M. Roché, D. Vigolo, L. N. Arnaudov, S. D. Stoyanov, T. D. Gurkov, G. G. Tsutsumanova, H. A. Stone, *Nat. Phys.* **2014**, *10*, 606; b) A. Zavabeti, J. Z. Ou, B. J. Carey, N. Syed, R. Orrell-Trigg, E. L. Mayes, C. Xu, O. Kavehei, A. P. O'mullane, R. B. Kaner, K. Kalantar-zadeh, T. Daeneke, *Science* **2017**, *358*, 332.

[12] Y. Wang, Y. Xia, *Nano Lett.* **2004**, *4*, 2047.

[13] J. Thelen, M. D. Dickey, T. Ward, *Lab Chip* **2012**, *12*, 3961.

[14] M. Dumke, T. Tombrello, R. Weller, R. Housley, E. Cirlin, *Surf. Sci.* **1983**, *124*, 407.

[15] Z. J. Farrell, C. Tabor, *Langmuir* **2018**, *34*, 234.

[16] J. Cutinho, B. S. Chang, S. Oyola-Reynoso, J. Chen, S. S. Akhter, I. D. Tevis, N. J. Bello, A. Martin, M. C. Foster, M. M. Thuo, *ACS Nano* **2018**, *12*, 4744.

[17] M. R. Khan, C. B. Eaker, E. F. Bowden, M. D. Dickey, *Proc. Natl. Acad. Sci. USA* **2014**, *111*, 14047.

[18] F. Magnan, J. Gagnon, F.-G. Fontaine, D. Boudreau, *Chem. Commun.* **2013**, *49*, 9299.

[19] C. B. Eaker, M. D. Dickey, *Appl. Phys. Rev.* **2016**, *3*, 031103.

[20] V. Sivan, S.-Y. Tang, A. P. O'Mullane, P. Petersen, N. Eshtiaghi, K. Kalantar-zadeh, A. Mitchell, *Adv. Funct. Mater.* **2013**, *23*, 144.

[21] a) C. Boyer, V. Bulmus, T. P. Davis, V. Ladmiral, J. Liu, S. Perrier, *Chem. Rev.* **2009**, *109*, 5402; b) T. Blin, A. Kakinen, E. H. Pilkington, A. Ivask, F. Ding, J. F. Quinn, M. R. Whittaker, P. C. Ke, T. P. Davis, *Polym. Chem.* **2016**, *7*, 1931.